Supporting Information for

Steric effect induces CO electroreduction to CH_4 on Cu–Au alloys

*Anxiang Guan,[a] Qihao Wang,[a] Yali Ji,[a] Si Li,[a] Chao Yang,[a] Linping Qian,[a] Lijuan Zhang,[a] Limin Wu,[b] Gengfeng Zheng[a,]**

[a]Laboratory of Advanced Materials, Department of Chemistry and Shanghai Key Laboratory of Molecular Catalysis & Innovative Materials, Faculty of Chemistry and Materials Science, Fudan University, Shanghai 200438, China.

[b]Department of Materials Science and State Key Laboratory of Molecular Engineering of Polymers, Fudan University, Shanghai 200438, China.

*Corresponding authors: Gengfeng Zheng

Email: gfzheng@fudan.edu.cn

Supplementary Methods

Electrochemical measurements

Electroreduction measurements were conducted on an Autolab PGSTAT30 (Netherlands) with a three-electrode flow cell at ambient conditions. A gas-diffusion electrode painted with IrO_2 catalyst (1 mg·cm^{-2}) and an Ag/AgCl (3 M KCl) were used as the counter and reference electrodes, respectively. A gas-diffusion electrode with a catalyst loading of 1 mg·cm^{-2} was used as working electrode. All applied potentials were converted into the reversible hydrogen electrode (RHE) scale by adding a value of (0.21 + 0.0591*pH) V. A KOH aqueous solution (1 M, pH 14) was served as the electrolyte. For the Faradaic efficiency analysis, gas and liquid products were quantified by in-line gas chromatograph (Shanghai Ramiin GC 2060) and ^{1}H NMR on Bruker AVANCEAV III HD 500, respectively.

DFT Calculations

Density functional theory (DFT) calculations were conducted using the Vienna *Ab initio* Simulation Package (VASP). The Perdew-Burke-Ernzerhof (PBE) and a supercell with a plane-wave basis sets (with a kinetic energy cutoff of 400 eV) was employed for the DFT calculations. The top two layers of the target model were set to be relaxed, and the rest several layers of the model were fixed. The final obtained energies were further corrected with the consideration of zero-point energy after geometry optimization for all intermediate states until the total energy of the system was stable with a 0.02 eV/Å force convergence.

Supplementary Figures

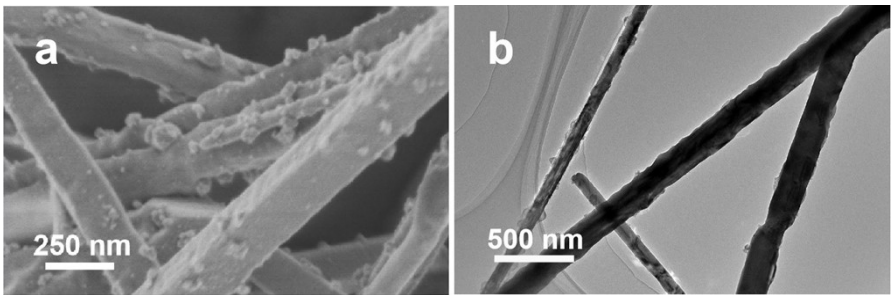

Fig. S1 High-resolution SEM image (a) and TEM image (b) of Cu nanowires.

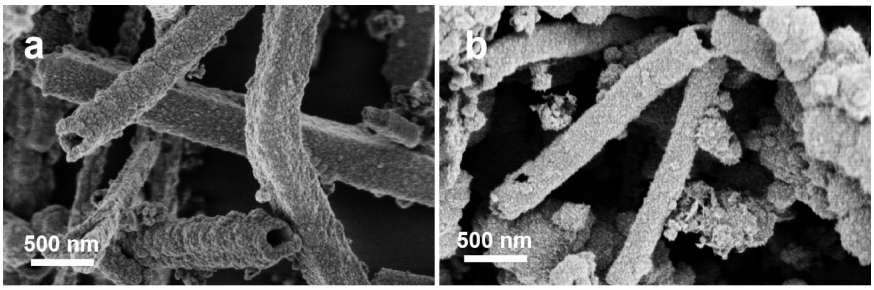

Fig. S2 The SEM images of (a) Cu_5Au and (b) CuAu alloy nanowires.

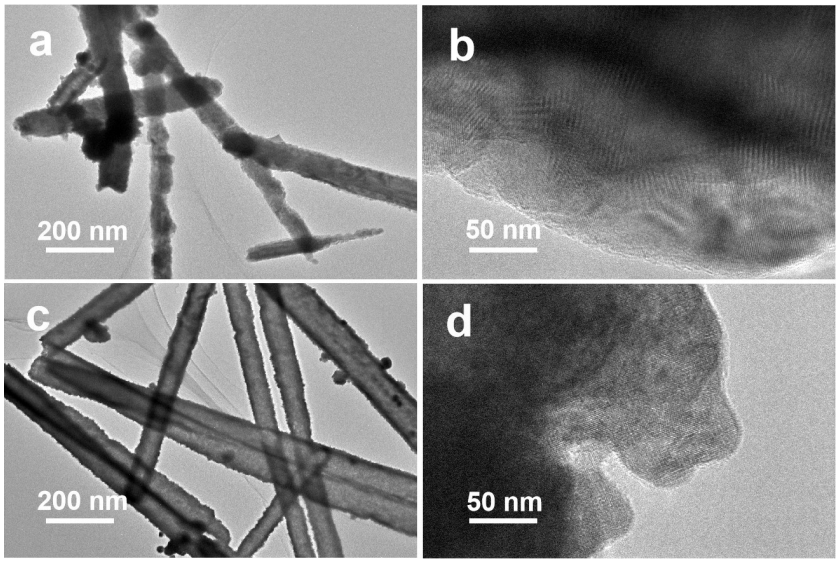

Fig. S3 Low- and high-resolution TEM images of (a, b) Cu_5Au and (c, d) CuAu alloy nanowires.

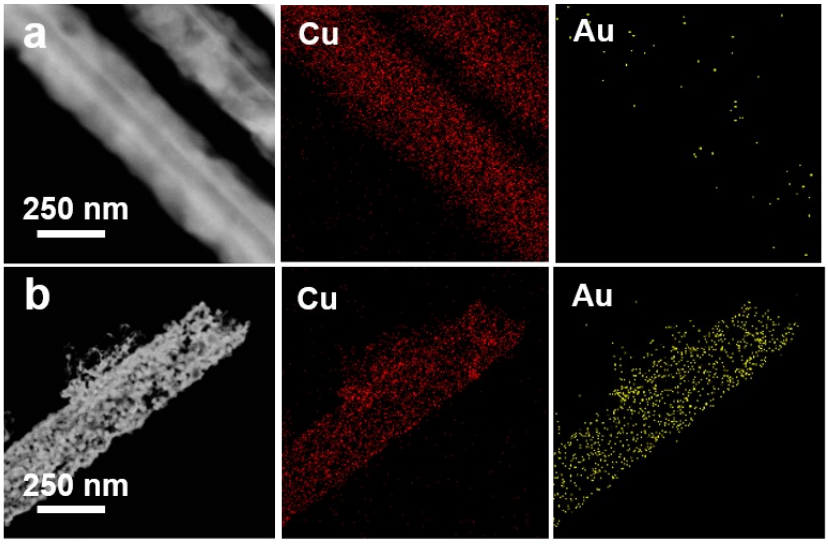

Fig. S4 EDS elemental mappings of (a) Cu_5Au and (b) CuAu alloy nanowires.

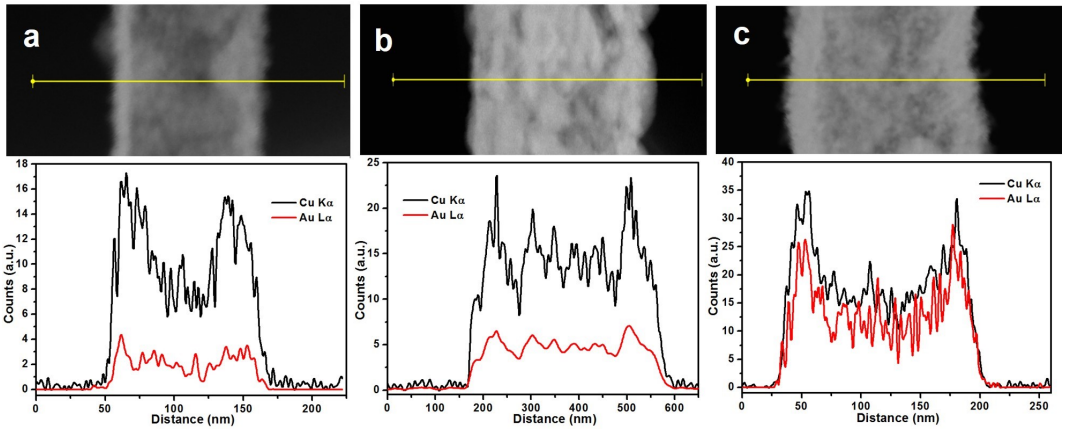

Fig. S5 Line scan analysis performed on (a) Cu_5Au, (b) Cu_3Au, and (c) CuAu alloy nanowires.

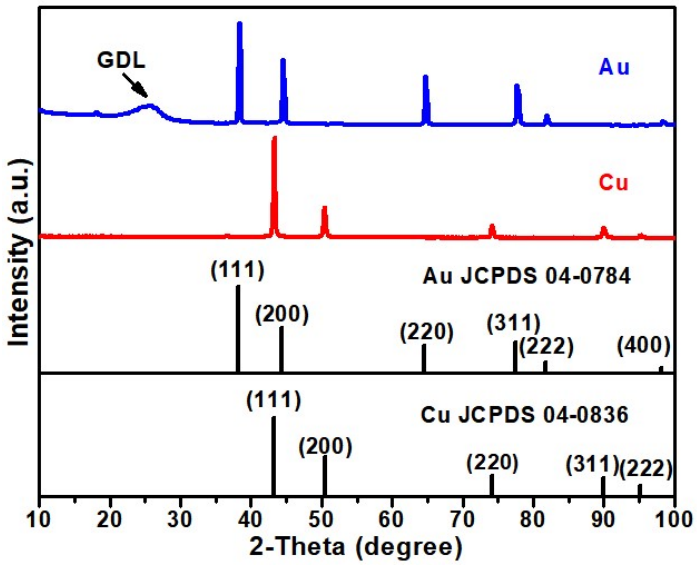

Fig. S6 XRD patterns of Cu and Au samples. The broad peak at 26° in the XRD pattern of Au was attributed to the characteristic peak of carbon-based gas-diffusion layer (GDL).

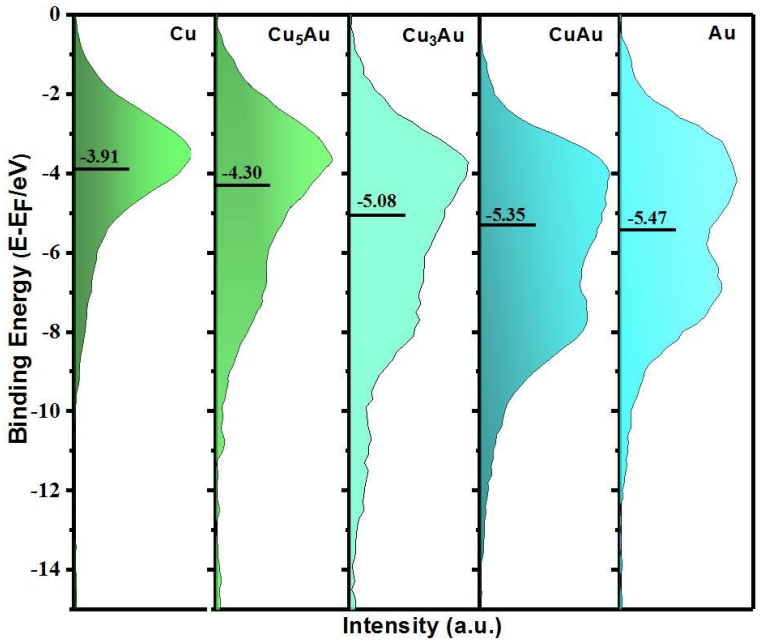

Fig. S7 Surface valence band photoelectron spectra of Cu, Au and Cu–Au alloy samples. The black bars indicated their d-band centers. For comparison, the lowest binding energy was set to −15 eV in binding energy.

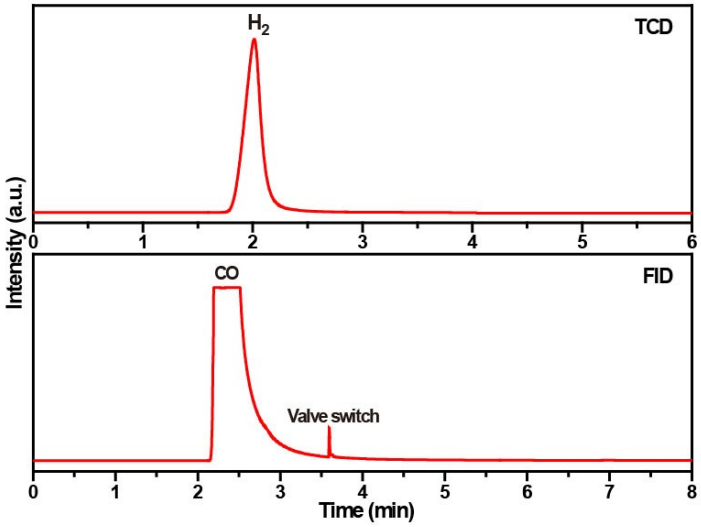

Fig. S8 Representative gas-chromatography spectra of gas products for CO electroreduction on Au catalyst.

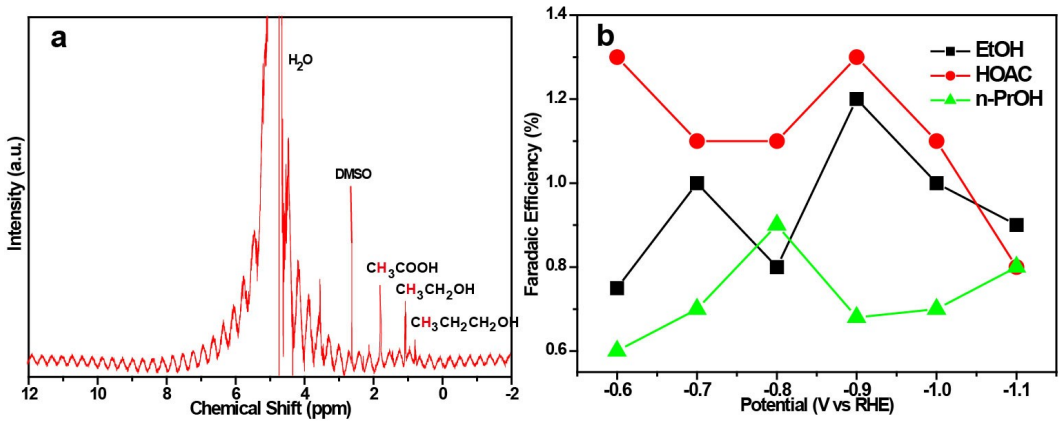

Fig. S9 (a) ^{1}H-NMR spectral data of liquid products for CO electroreduction on Au catalyst (The signal of ^{1}H-NMR was derived from the hydrogen atoms highlighted in red), (b) Faradaic efficiencies of liquid products for CO electroreduction on Au catalyst.

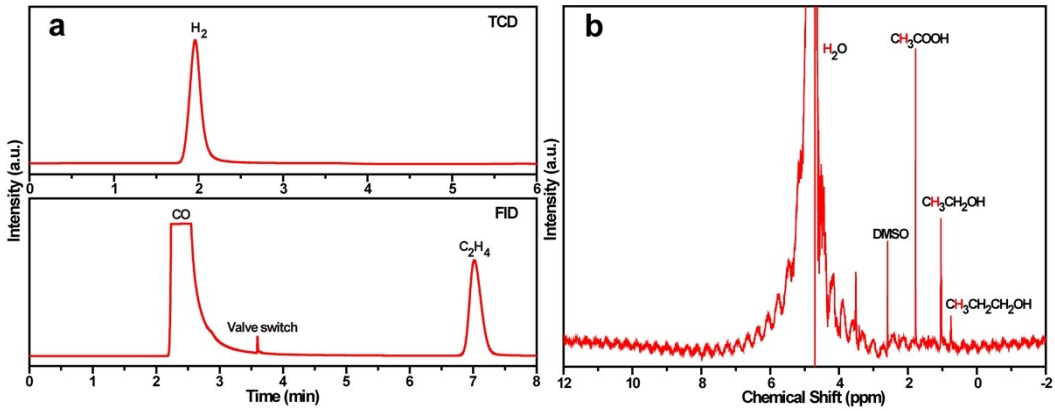

Fig. S10 (a) Representative gas-chromatography spectra of gas products, and (b) ^{1}H-NMR spectral data of liquid products for CO electroreduction on Cu nanowire catalyst (The signal of ^{1}H-NMR was derived from the hydrogen atoms highlighted in red).

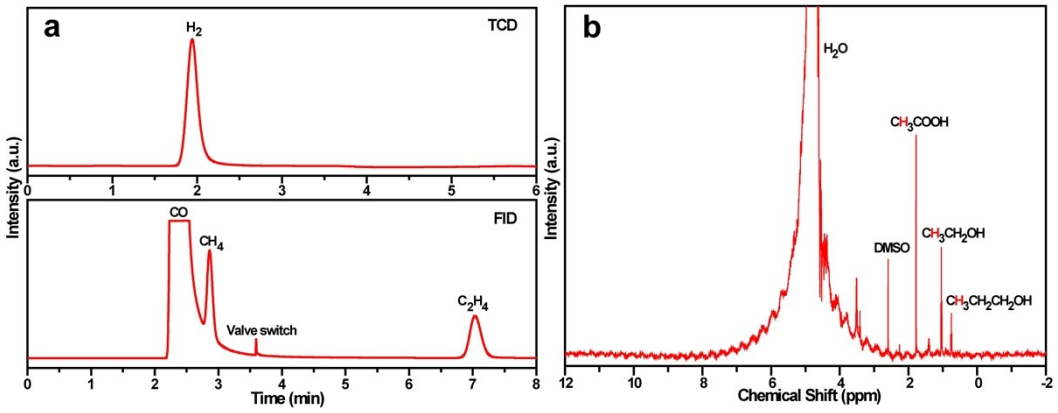

Fig. S11 (a) Representative gas-chromatography spectra of gas products, and (b) ^{1}H-NMR spectral data of liquid products for CO electroreduction on Cu_3Au nanowire catalyst (The signal of ^{1}H-NMR was derived from the hydrogen atoms highlighted in red).

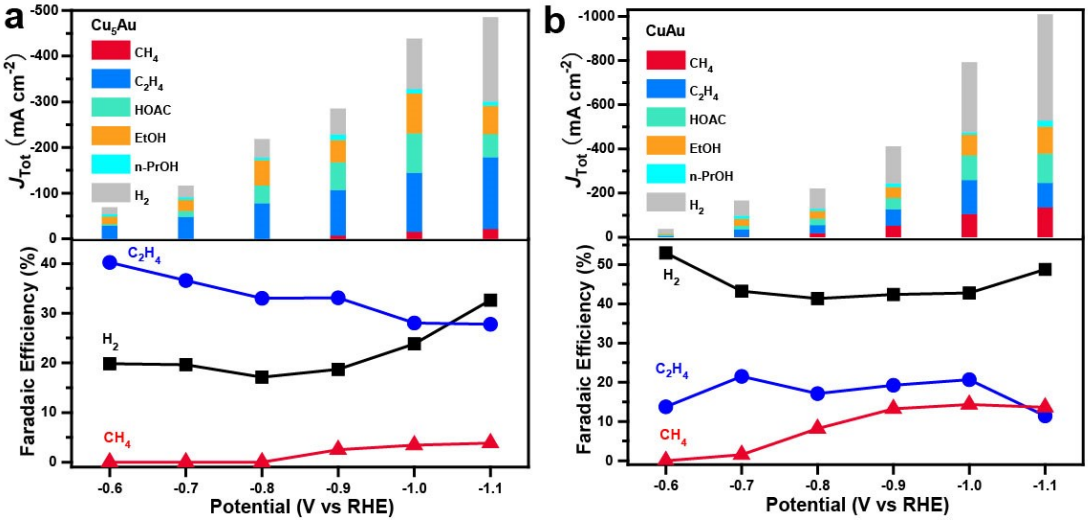

Fig. S12 CO electroreduction performance of the (a) Cu_5Au and (b) CuAu alloy catalysts. Top panels: partial current densities with respect to different products. Bottom panels: Faradaic efficiencies of H_2, C_2H_4 and CH_4.

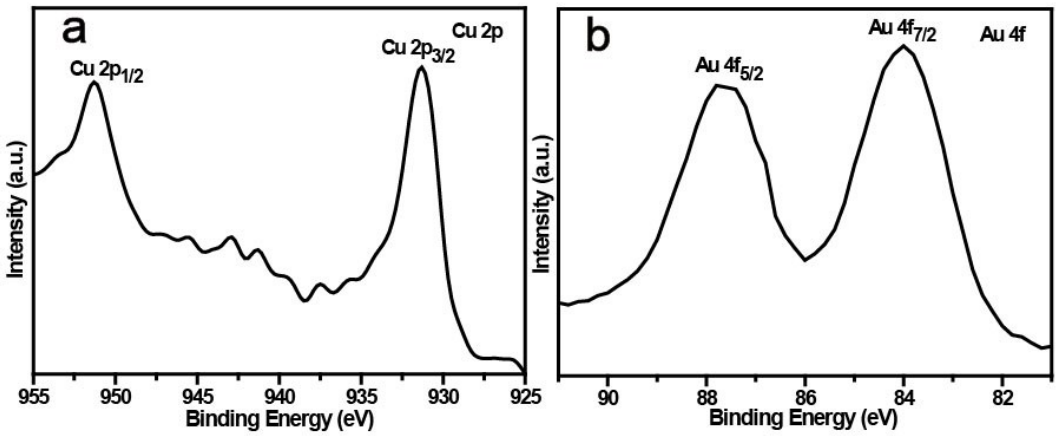

Fig. S13 (a) Cu 2p and (b) Au 4f XPS spectra of Cu_3Au after CO electroreduction.

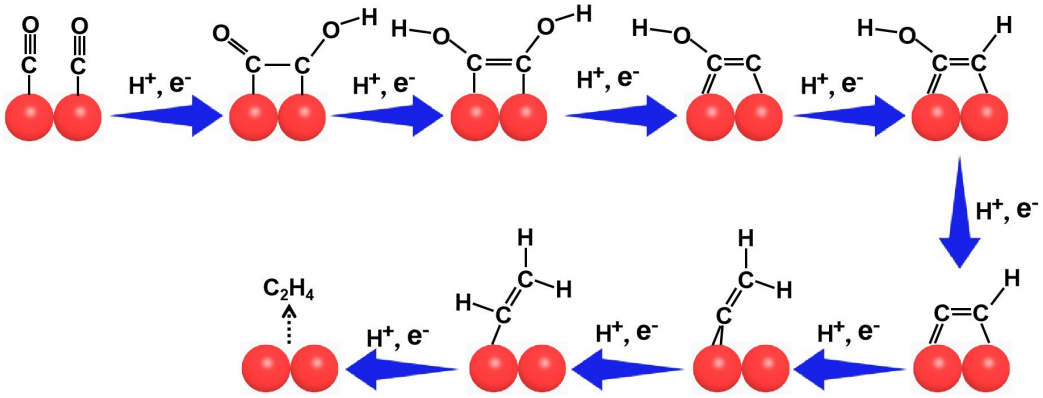

Fig. S14 The formation mechanism of C_2H_4 on the Cu surface. The red spheres were denoted as Cu atoms

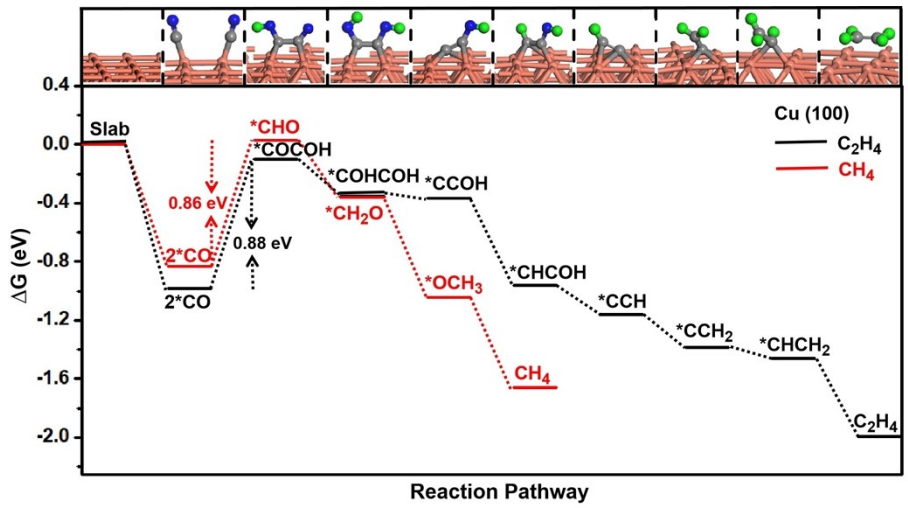

Fig. S15 Free energy profiles for C_2H_4 and CH_4 generation over Cu (100). The grey, blue and green spheres were denoted as C, O and H atoms, respectively.

Table S1. Elemental content in different samples determined by ICP-OES

Sample ID	Element	Reported Conc. (mg/L)	Amount of substance (mol)	Molar ratio of Cu : Au
Cu_5Au	Cu	3.66	0.058	4.83:1
	Au	2.27	0.012	
Cu_3Au	Cu	2.81	0.044	2.93:1
	Au	3.01	0.015	
CuAu	Cu	1.84	0.029	1.04:1
	Au	5.50	0.028	